Insights into the Zonal-Mean Response of the Hydrologic Cycle to Global Warming from a Diffusive Energy Balance Model

NICHOLAS SILER

College of Earth, Ocean, and Atmospheric Sciences, Oregon State University, Corvallis, Oregon

GERARD H. ROE

Department of Earth and Space Sciences, University of Washington, Seattle, Washington

KYLE C. ARMOUR

School of Oceanography and Department of Atmospheric Sciences, University of Washington, Seattle, Washington

(Manuscript received 13 February 2018, in final form 25 May 2018)

ABSTRACT

Recent studies have shown that the change in poleward energy transport under global warming is well approximated by downgradient transport of near-surface moist static energy (MSE) modulated by the spatial pattern of radiative forcing, feedbacks, and ocean heat uptake. Here we explore the implications of downgradient MSE transport for changes in the vertically integrated moisture flux and thus the zonal-mean pattern of evaporation minus precipitation ($E - P$). Using a conventional energy balance model that we have modified to represent the Hadley cell, we find that downgradient MSE transport implies changes in $E - P$ that mirror those simulated by comprehensive global climate models (GCMs), including a poleward expansion of the subtropical belt where $E > P$, and a poleward shift in the extratropical minimum of $E - P$ associated with the storm tracks. The surface energy budget imposes further constraints on E and P independently: E increases almost everywhere, with relatively little spatial variability, while P must increase in the deep tropics, decrease in the subtropics, and increase in middle and high latitudes. Variations in the spatial pattern of radiative forcing, feedbacks, and ocean heat uptake across GCMs modulate these basic features, accounting for much of the model spread in the zonal-mean response of E and P to climate change. Thus, the principle of downgradient energy transport appears to provide a simple explanation for the basic structure of hydrologic cycle changes in GCM simulations of global warming.

1. Introduction

In the zonal and annual mean, Earth's atmosphere transports energy down the meridional insolation gradient, from the tropics to higher latitudes. Consequently, the climate is much more temperate than it would be if radiative equilibrium were imposed at each latitude (e.g., Hartmann 1994; Pierrehumbert 2010).

The dominant mechanisms of atmospheric energy transport vary by region. Outside the tropics, most poleward energy transport is accomplished by midlatitude eddies (both stationary and transient), which transport moist, warm, tropical air poleward and cool, dry, polar air equatorward. In the tropics, by contrast, poleward energy transport is primarily accomplished by the Hadley cell, whose total energy transport is a small residual of offsetting contributions from its lower (equatorward) and upper (poleward) branches (e.g., Hartmann 1994). Because the tropical atmosphere is weakly stable, moist static energy increases with height, and thus energy transport is slightly larger within the upper branch of the Hadley cell, resulting in poleward transport overall. This constraint has proven fundamental to understanding important aspects of the Hadley cell's behavior, including its seasonality (e.g., Donohoe et al. 2013) and its hemispheric asymmetry as a consequence of cross-equatorial ocean heat transport (Frierson et al. 2013; Marshall et al. 2014).

Atmospheric energy transport is also closely tied to the hydrologic cycle, as shown in Fig. 1. One form of atmospheric energy transport is the latent heat of

Corresponding author: Nicholas Siler, nick.siler@oregonstate.edu

DOI: 10.1175/JCLI-D-18-0081.1

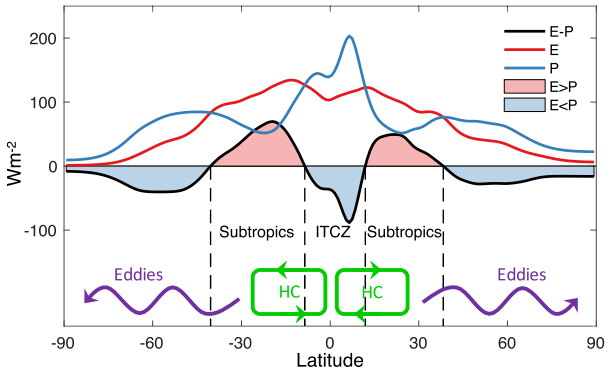

FIG. 1. The $E - P$ (black line) from ERA-Interim, averaged over the 35-yr period from 1981 to 2010 (scaled by L to have units of W m^{-2}), also E (red line) and P (blue line). Red shading indicates subtropical latitudes where $E > P$, implying a net divergence of atmospheric latent heat transport. Blue shading indicates latitudes where $P > E$, which includes the ITCZ. The profile of $E - P$ is the result of poleward latent heat transport by midlatitude eddies (indicated schematically in purple) and equatorward latent heat transport within the lower branch of the HC (green).

moisture, the divergence of which is proportional to evaporation minus precipitation at the surface ($E - P$; black line in Fig. 1). Outside the tropics, latent heat is transported downgradient by eddies, resulting in net divergence (and thus $E - P > 0$) in the subtropics and net convergence (and thus $E - P < 0$) at higher latitudes. In contrast, the Hadley cell transports latent heat upgradient as a result of equatorward flow at low levels, where water vapor is concentrated. Such upgradient transport leads to strong convergence of latent heat near the equator [known as the intertropical convergence zone (ITCZ)], and adds to the latent heat divergence in the subtropics. Because E is constrained by net surface radiation, which has relatively little spatial structure, it varies weakly with latitude (Fig. 1, red line). The undulations in $E - P$ are thus mirrored in P (Fig. 1, blue line), explaining why deserts are largely confined to the subtropics, while the deep tropics are home to many of the wettest places on Earth.

The principle of downgradient energy transport by the atmosphere has given rise to the widespread use of energy balance models (EBMs) to study the zonal-mean climate. The theoretical basis for EBMs comes from the fact that, on long time scales, the zonal-mean net heating of the atmosphere Q_{net} must be balanced by the divergence of northward column-integrated atmospheric energy transport F:

$$Q_{\text{net}}(x) = \frac{1}{2\pi a^2}\frac{dF}{dx}, \tag{1}$$

where a is the radius of Earth, x is the sine of latitude, and Q_{net} is the difference between the net downward energy flux at the top of the atmosphere (TOA) and the surface (e.g., Pierrehumbert 2010). In most early EBMs (Budyko 1969; North 1975), F was assumed to be proportional to the meridional gradient in near-surface temperature T. However, recognizing that T represents only the sensible component of atmospheric heat content, more recent EBM formulations have replaced T with near-surface moist static energy $h = c_pT + Lq$, where c_p is the specific heat of air, L is the latent heat of vaporization, and q is the near-surface specific humidity[1] (e.g., Flannery 1984; Frierson et al. 2007; Hwang and Frierson 2010; Rose et al. 2014; Roe et al. 2015). In the continuous limit, energy transport in the moist static EBM is governed by Fickian diffusion

$$F(x) = -\frac{2\pi p_s}{g} D(1 - x^2)\frac{dh}{dx}, \tag{2}$$

where p_s is surface air pressure (1000 hPa), g is the acceleration due to gravity, D is a (constant) diffusion coefficient (with units of m^2 s^{-1}), and $(1 - x^2)$ accounts for the spherical geometry. Typically, relative humidity is assumed to be fixed at 80%, making h a single-valued function of T (Hwang and Frierson 2010; Rose et al. 2014; Roe et al. 2015). While unrealistic over land, this value is close to the observed near-surface relative humidity over the oceans, where most eddy heat transport occurs (Peixoto and Oort 1996). Finally, combining Eqs. (1) and (2) yields a single expression for the moist static energy balance model (MEBM) that relates Q_{net} directly to h (and thus T):

$$Q_{\text{net}}(x) = -\frac{p_s}{ga^2} D\frac{d}{dx}\left[(1 - x^2)\frac{dh}{dx}\right]. \tag{3}$$

The MEBM defined in Eq. (3) has proven to be remarkably successful at emulating the climate response to anthropogenic forcing simulated by comprehensive global climate models (GCMs). For example, Hwang and Frierson (2010) showed that the MEBM successfully predicts the increase in midlatitude poleward heat transport with global warming, and found that the intermodel differences in heat transport can be explained by the MEBM as a result of differences in climate feedbacks. More recent studies have also found that the MEBM realistically emulates the surface temperature response to different spatial patterns of ocean heat uptake (Rose et al. 2014) and climate feedbacks (Roe et al. 2015) across a range of GCMs.

[1] Note that this definition of h neglects geopotential, which is close to zero near the surface.

Despite these successes, the MEBM has an important limitation: it does not correctly simulate latent heat transport, which is upgradient within the Hadley cell. To address this limitation, here we incorporate a simple Hadley cell parameterization into the MEBM, which allows latent heat to travel upgradient even while total energy transport is downgradient, thus permitting a more realistic representation of the hydrologic cycle. In section 2, we show that the modified MEBM is able to reproduce the basic pattern of $E - P$ in the climatology of both observations and climate models. In section 3, we use the modified MEBM to study the zonal-mean response of $E - P$ to global warming, giving special attention to how the MEBM solution differs from the well-known thermodynamic scaling argument of Held and Soden (2006). We show that the MEBM captures important aspects of the change in $E - P$ in GCM simulations, including the poleward expansion of the subtropics and the poleward shift in the midlatitude storm tracks. When driven by the spatial patterns of forcing, feedbacks, and ocean heat uptake corresponding to individual GCMs, the MEBM also captures much of the intermodel variability in the response of $E - P$ to climate change. Finally, using our recent formulation for the dependence of evaporation on surface temperature and ocean heat uptake (Siler et al. 2018), we disaggregate the individual contributions of P and E, and show that each reproduces many of the features seen in climate models.

2. The modified MEBM and its climatology

Figure 2a shows annual-mean $Q_{\text{net}}(x)$ calculated from ERA-Interim over the period 1981–2010. From Eq. (1), positive values of Q_{net} in the tropics indicate net divergence of atmospheric heat transport, while negative values at higher latitudes indicate net convergence. Inserting this Q_{net} profile into Eq. (3), we then choose a value of D so that $T(x)$ resembles the observed zonal-mean 2-m air temperature at sea level. The best agreement is found by setting $D = 1.16 \times 10^6\,\text{m}^2\,\text{s}^{-1}$ (Fig. 2b), which is within 10% of the value used in previous studies (Hwang and Frierson 2010; Rose et al. 2014; Roe et al. 2015). Like these studies, we assume that D is uniform with latitude and held fixed at this value for all following analyses.

To give the MEBM a realistic hydrologic cycle, we must alter the partitioning between latent and dry static heat transport within the tropics, where latent heat transport is upgradient. This idea originated with Sellers (1969), whose primitive 10-box EBM included the advection of latent and sensible heat by the mean meridional wind, which he fit to observations. We seek a less ad hoc approach, using Eqs. (1)–(3) and a few additional constraints to solve for the meridional circulation and its associated latent heat transport.

Our first step is to use a weighting function $w(x)$ to partition the total heat transport into Hadley cell (HC) and eddy components

$$F_{\text{HC}}(x) = w(x)F(x) \quad \text{and} \tag{4}$$

$$F_{\text{eddy}}(x) = [1 - w(x)]F(x). \tag{5}$$

For $w(x)$, we choose a Gaussian function

$$w(x) = \exp\left(\frac{-x^2}{\sigma_x^2}\right), \tag{6}$$

and specify a characteristic width of $\sigma_x = 0.3$, resulting in the profile shown in Fig. 2c. With this choice, eddies account for essentially all energy transport poleward of 45° latitude, while the Hadley cell accounts for most energy transport inside of 15° latitude (and 100% at the equator). Note that the original MEBM is recovered by setting $w(x) = 0$ (dashed red line in Fig. 2c).

There are two obvious limitations to Eq. (6). First, because $w(x)$ approaches zero outside the tropics, it does not account for heat transport by the Ferrel and polar cells, which comprise the extratropical components of the mean meridional circulation. Second, by choosing a fixed value for σ_x, we neglect possible changes in the partitioning between eddy and Hadley cell transport in response to global warming. In efforts to address these limitations, we have experimented with various other representations of $w(x)$, but have generally found that any gains in realism come with increased complexity, and do not change the essence of the climate response. In our view, Eq. (6) seems to strike an appropriate balance between simplicity and realism.

Having quantified the total energy transported by the Hadley cell [Eq. (4)], its circulation can then be determined following Held (2001). Let $\psi(x)$ be the southward mass transport in the lower branch of the cell, which by mass conservation is equal to the northward mass transport in the upper branch. Then

$$F_{\text{HC}}(x) = \psi(x)g(x), \tag{7}$$

where $g(x)$ is the gross moist stability of the atmosphere, which represents the flow-weighted difference in moist static energy between the upper and lower branches at each latitude (Neelin and Held 1987). In the tropical upper troposphere, temperature gradients tend to be small, and moist static energy is relatively uniform. As a result, variations in $g(x)$ are primarily caused by variations in $h(x)$, implying that

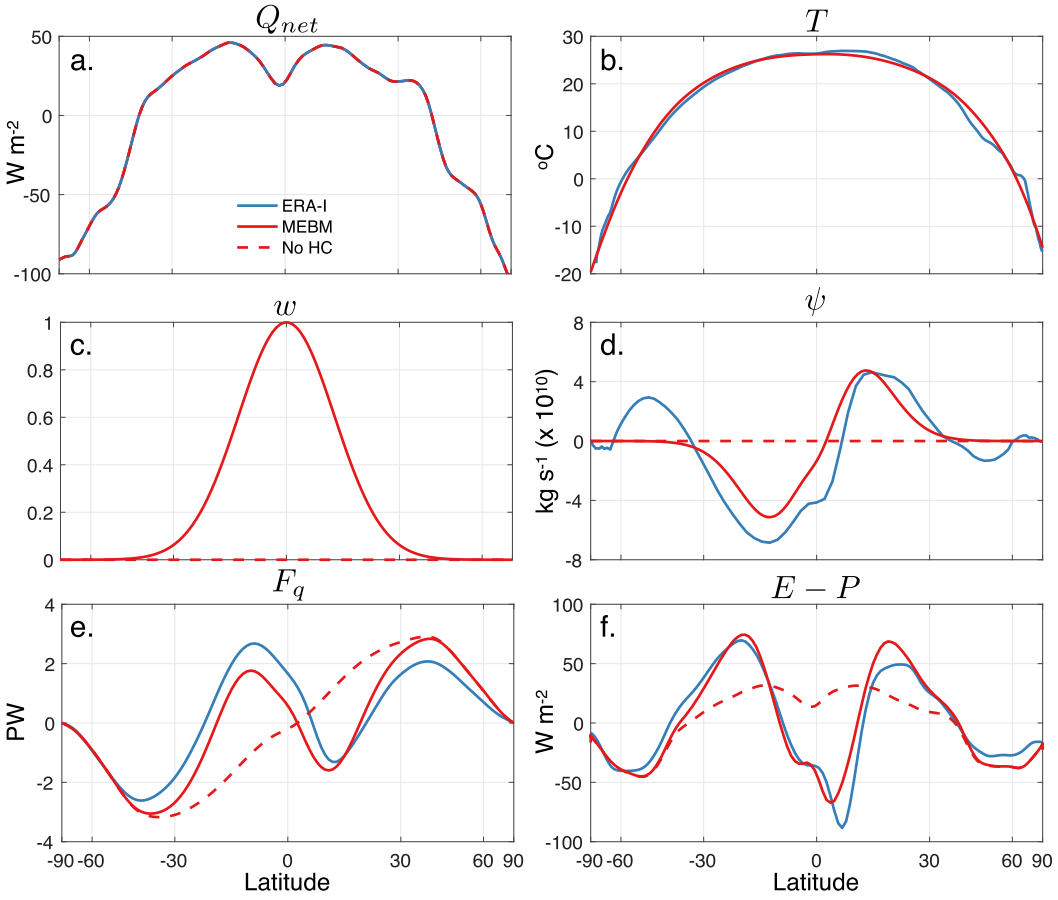

FIG. 2. (a) The Q_{net} calculated from ERA-Interim over the period 1981–2010, which is equal to the net downward radiative flux at the TOA minus ocean heat uptake. The x axis is area-weighted, and is therefore linear in x, the sine of latitude. (b) Zonal-mean air temperature at sea level from ERA-Interim (blue) and the MEBM (red), with $D = 1.16 \times 10^6\,\text{m}^2\,\text{s}^{-1}$. (c) A weighting function representing the fraction of total atmospheric energy transport in the MEBM that is performed by the HC. The dashed red line at $w = 0$ shows the weighting function implicit in the original MEBM with no HC. (d) The southward mass transport within the lower branch of the mean meridional circulation in ERA-Interim (blue line), the modified MEBM (solid red line), and the original MEBM (dashed red line). In ERA-Interim, this value applies to the layer below 900 hPa, where most atmospheric water vapor is concentrated, and includes contributions from the Ferrel and polar cells in addition to the HC. (e) As in (d), but for the northward latent heat transport by the atmosphere. (f) As in (d), but for $E - P$, which is equal to the divergence of northward latent heat transport in (e).

$$g(x) \approx h_T - h(x), \tag{8}$$

where h_T represents the (spatially uniform) moist static energy in the tropical upper troposphere (Held 2001; Merlis et al. 2013; Hill et al. 2015). We set $h_T = 1.06 \times h(0)$, or 6% above the near-surface moist static energy at the equator, which results in the best agreement with observed moisture transport, and is a reasonable approximation of the equatorial moist static energy profile in reanalysis. With h_T specified, we then solve for $\psi(x)$ from Eqs. (4) and (7) (Fig. 2d).

Since $g(0) > 0$, the net transport of moist static energy is downgradient throughout the Hadley cell. However, because the upper branch of the cell is essentially dry, latent heat transport F_q is confined to the lower branch, implying that

$$F_{\text{HC},q}(x) = -\psi(x) L q(x). \tag{9}$$

Combining the latent heat transport by the Hadley cell with the downgradient eddy contribution in the extratropics gives the total latent heat transport $F_q(x)$ (Fig. 2e). Finally, the divergence of $F_q(x)$ gives $E - P$ (Fig. 2f).

Figure 3 shows the same MEBM solutions for T and $E - P$ as in Figs. 2b and 2f, but now based on the average Q_{net} profile among GCM simulations of the preindustrial climate from the latest Coupled Model

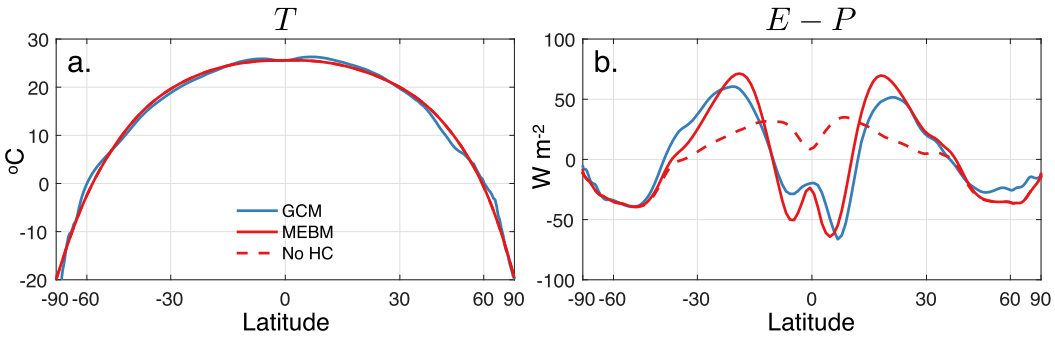

FIG. 3. As in Figs. 2b,f, but for the ensemble mean of 20 CMIP5 simulations of the preindustrial climate (blue line). The MEBM solution was computed exactly as for Fig. 2, but using the Q_{net} profile from the CMIP5 ensemble.

Intercomparison Project (CMIP5). The variables in Fig. 3 were computed exactly as described above (i.e., with the same value of D and Hadley cell parameters), so that the differences between Figs. 2 and 3 are entirely due to differences in Q_{net}. In both Figs. 2 and 3, dashed red lines show the MEBM solution without a Hadley cell [i.e., $w(x) = 0$].

Figures 2 and 3 show that the Hadley cell version of the MEBM is a significant improvement over the original MEBM. Based on a simple diffusive representation of downgradient energy transport, it successfully emulates the basic structure of the zonal-mean hydrologic cycle in both reanalysis and GCM simulations. In particular, the MEBM captures the minima in $E - P$ associated with the ITCZ and midlatitude storm tracks, and also provides a reasonable estimate of the latitudes where $E - P = 0$, which mark the boundaries of the subtropics (Fig. 1). And despite some discrepancies in $E - P$ in the tropics, the MEBM correctly produces the double ITCZ evident in CMIP5 models, and the single ITCZ north of the equator in observations. This result adds further support to the growing consensus that hemispheric asymmetries in Q_{net}, and required cross-equatorial heat transport, play a leading role in setting the location of the ITCZ (Kang et al. 2008; Frierson and Hwang 2012; Frierson et al. 2013; Hwang and Frierson 2013; Hwang et al. 2013; Donohoe et al. 2013, 2014; Marshall et al. 2014).

A summary of energy transports in the modified MEBM is given in Table 1, with columns representing the eddy (F_{eddy}) and Hadley cell (F_{HC}) contributions and rows representing the latent heat (F_q) and dry static energy (F_T) contributions. The sum of all four terms is equal to the total energy transport, which is downgradient and set by Eq. (2) with constant diffusivity and relative humidity. In the extratropics, where eddy transport dominates (i.e., $w \approx 0$), F_q and F_T are both diffusive. In the tropics, however, F_q is upgradient within the lower branch of the Hadley cell. We have shown that this modification allows the MEBM to reproduce the broad structure of the zonal-mean hydrologic cycle in both GCMs and reanalysis. In the next section, we use the modified MEBM to explore the implications of downgradient energy transport for how the zonal-mean hydrologic cycle responds to global warming.

3. Global warming simulations

In section 5 of their seminal paper on the response of the hydrologic cycle to global warming, Held and Soden (2006, hereinafter HS06) consider the implications of downgradient energy transport for the change in zonal-mean $E - P$. Conceptualizing the transport response as diffusive, they argue that, because of relatively weak gradients in the spatial pattern of warming, the pattern of $E - P$ should amplify with surface warming at a rate roughly equal to

$$\frac{E' - P'}{E - P} \approx \alpha T', \tag{10}$$

where primes indicate the difference between the warmed and mean-state climates and

$$\alpha = \frac{L}{R_v T^2} \tag{11}$$

is the Clausius–Clapeyron scaling factor, with R_v representing the gas constant of water vapor.

TABLE 1. (top) Northward latent and (bottom) dry static energy transport by the (left) eddies and (right) HC in the MEBM. The sum of all four terms is equal to the total energy transport $F(x)$ [Eq. (2)].

	Eddies	Hadley cell
$F_q(x)$	$-\frac{2\pi p_s}{g} D(1-x^2) L \frac{dq}{dx}[1 - w(x)]$	$-\psi(x) L q(x)$
$F_T(x)$	$-\frac{2\pi p_s}{g} D(1-x^2) c_p \frac{dT}{dx}[1 - w(x)]$	$\psi(x)[g(x) + L q(x)]$

HS06 found that Eq. (10) broadly captured the magnitude and spatial pattern of $E' - P'$ predicted in GCM simulations of global warming. However, they also identified robust aspects of $E' - P'$ in GCMs that Eq. (10) did not explain, including a poleward expansion of the subtropics, where $E - P > 0$, and a poleward shift of the $E - P$ minimum associated with the midlatitude storm tracks. Equation (10) also provides limited insight into the differences in $E' - P'$ across GCMs.

Here we build on HS06's diffusive interpretation of hydrologic change in three ways. First, in section 3a, we use the MEBM to simulate $E' - P'$ in response to a spatially uniform forcing and feedback. In contrast to the HS06 approximation, we find that diffusive energy transport does in fact predict subtropical expansion and a poleward shift in the storm tracks. These features of the hydrologic response are found to be directly related to polar-amplified warming, which the HS06 approximation does not take into account. In section 3b, we examine the MEBM response with the full patterns of forcing, feedbacks, and ocean heat uptake taken from individual CMIP5 models, and find that the MEBM captures much of the overall structure of $E' - P'$ in the ensemble mean, and most of the variability in $E' - P'$ patterns across models. Finally, in section 3c, we use surface energy constraints to solve for E' and P' independently, and find that these solutions also compare well with GCMs. Together, these results suggest that diffusive energy transport may provide greater insight into zonal-mean hydrologic change than previously recognized.

a. *Implications of diffusive energy transport for $E' - P'$ in the presence of polar amplification*

Let $R_f(x)$ be defined as the TOA radiative forcing resulting from an abrupt quadrupling of atmospheric CO_2, and $G'(x)$ be defined as the change in ocean heat uptake. Following the linear feedback framework of Roe et al. (2015), the perturbation form of the MEBM can then be expressed as

$$R_f(x) - G'(x) + \lambda(x)T'(x) = \frac{1}{2\pi a^2}\frac{dF'}{dx}, \qquad (12)$$

where $\lambda(x)$ is the strength of the local climate feedback, and $F'(x)$ is the change in atmospheric heat transport, which in the MEBM is given by

$$F'(x) = -\frac{2\pi p_s}{g} D(1 - x^2)\frac{dh'}{dx}, \qquad (13)$$

where $h'(x) = c_p T'(x) + Lq'(x)$ represents the perturbation near-surface moist static energy.

Because $q' \approx \alpha T' q$ under constant relative humidity (according to a linearization of the Clausius–Clapeyron equation), the solution to Eqs. (12) and (13) will depend to some extent on the reference climate, which we define here to be the MEBM solution from reanalysis (Fig. 2, red lines). As in the mean-state MEBM, we assume that $h'_T = 1.06 \times h'(0)$, implying a modest increase in gross moist stability at the equator. We also assume that D in Eq. (13) is unchanged from the mean-state diffusion coefficient. Combining Eqs. (12) and (13) yields a single differential equation that we solve numerically for $T'(x)$ given $R_f(x)$, $G'(x)$, and $\lambda(x)$. The solution for $E' - P'$ then follows from T', just as described for the mean-state climate in section 2.

For the first part of this analysis, we assume that $G' = 0$ and that R_f and λ are spatially uniform, with values of $8\,\mathrm{W\,m^{-2}}$ and $-1.5\,\mathrm{W\,m^{-2}\,K^{-1}}$, respectively. These values are typical of the global means found in simulations of abrupt CO_2 quadrupling, which we discuss in section 3b.

Figure 4a shows the pattern of warming given by the MEBM in response to this uniform forcing and feedback. In agreement with previous studies of the MEBM response to radiative forcing (Roe et al. 2015), Fig. 4a shows significantly more warming at high latitudes than in the tropics. Since R_f, λ, and G' are all spatially uniform, such polar amplification of surface warming in the MEBM can only result from the nonlinearity of the Clausius–Clapeyron equation, which dictates that water vapor will increase most in warm regions, causing an increase in the meridional gradient of latent heat, and thus an increase in the rate of latent heat transport from the tropics to the poles.

The $E' - P'$ profile implied by this pattern of warming is given in Fig. 4b (solid red line), along with the HS06 approximation from Eq. (10) (blue line), which represents an amplification of the mean-state $E - P$ profile. Comparing the two curves, three differences stand out:

1) The magnitude of $E' - P'$ is generally weaker in the MEBM than in the HS06 approximation, particularly outside the tropics.
2) The MEBM shows an expansion of the subtropical region where $E - P > 0$ (Fig. 4, vertical green lines), whereas HS06 simply amplifies the existing spatial pattern of $E - P$.
3) The MEBM places the extratropical minimum of $E' - P'$ poleward of its climatological position (Fig. 4, vertical purple lines). This minimum corresponds to the latitude of maximum moisture convergence, the poleward shift of which is commonly attributed to a shift in the latitude of the midlatitude storm tracks.

As we will show, each of these differences stems from the modification of poleward heat transport by polar amplification in the MEBM, which HS06 did not take into account. To explain why, it is convenient to revert to

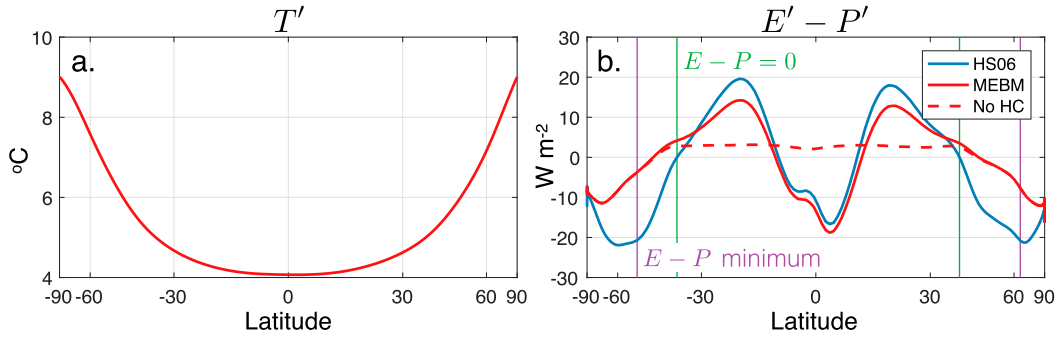

FIG. 4. (a) The change in zonal-mean surface temperature in the MEBM in response to a spatially uniform radiative forcing and feedback. (b) The change in $E - P$ from the MEBM (red) and the HS06 approximation [blue; Eq. (10)]. The dashed red line represents the MEBM solution with no HC [i.e., $w(x) = 0$]. The HS06 approximation is calculated using the MEBM warming profile from (a), but does not account for the impact of polar amplification on poleward heat transport. The vertical green lines indicate the highest latitude where $E - P = 0$ in the mean-state MEBM solution (Fig. 2f), which is a rough measure of the subtropical boundary. The vertical purple lines indicate the extratropical minimum in mean-state $E - P$, which is related to the mean-state position of the storm tracks.

the more primitive version of the MEBM in which latent heat is fluxed downgradient everywhere (Fig. 4b, dashed red line). While this version gives the wrong hydrologic cycle in the tropics, its profile of $E' - P'$ is nearly equivalent to the Hadley cell version of the MEBM poleward of about 40° latitude, where the HS06 approximation is most different from the MEBM solution. In the primitive MEBM, the perturbation northward latent heat transport is approximately given by

$$F_q'(x) \approx \beta F_q(x), \tag{14}$$

where

$$\beta = \frac{dT'/dx}{dT/dx} + \left(\alpha - \frac{2}{T}\right) T' \tag{15}$$

represents the fractional change in $F_q(x)$ (see the appendix for derivation). Then $E' - P'$ is equal to the divergence of $F_q'(x)$, and comprises two distinct terms:

$$E' - P' = \overbrace{\beta(E - P)}^{\text{Term 1}} + \overbrace{\frac{1}{2\pi a^2} F_q \frac{d\beta}{dx}}^{\text{Term 2}}. \tag{16}$$

Equation (14) implies that the profile of latent heat transport is amplified under global warming by a factor of $\beta(x)$. If warming were spatially uniform, $F_q(x)$ would scale at close to the Clausius–Clapeyron rate of $\alpha T'$, and $E - P$ would scale at a similar rate because term 2 in Eq. (16) would be small, owing to weak meridional variations in $\alpha - 2/T$. Thus, if T' were spatially uniform, the MEBM solution for $E' - P'$ would be consistent with the approximation of HS06 [Eq. (10)].

In reality, however, T' increases with latitude (Fig. 4a), which impacts the hydrologic cycle in two ways. First, by weakening the meridional temperature gradient, polar amplification decreases β everywhere [first term in Eq. (15)], and thus partially offsets the increase in F_q from the Clausius–Clapeyron effect. This partly explains the lower magnitude of $E - P$ amplification in the MEBM compared to the HS06 approximation, but does not explain the poleward shift of $E - P$ in the MEBM.

Second, because of the weak temperature dependence of α, the second term in Eq. (15) increases almost linearly with T', implying a larger value of β (and thus a larger fractional increase in F_q) at high latitudes. In terms of the hydrologic cycle, the increase in β with latitude contributes to an increase in $E' - P'$ everywhere, but especially in the midlatitudes where F_q is greatest [Eq. (16), term 2]. In the subtropics, this positive contribution to $E' - P'$ results in an expansion of the region where $E - P > 0$, and thus a poleward shift in the latitude where $E - P = 0$. Farther poleward, the magnitude of this positive $E' - P'$ contribution decreases with latitude in rough proportion to F_q. This implies a larger (smaller) contribution equatorward (poleward) of the extratropical $E - P$ minimum, and thus a poleward shift in the latitude where this minimum occurs.

A second perspective on how polar amplification alters the spatial pattern of $E - P$ comes from the global water budget. Like F_q (Table 1), F_q' can be separated into eddy and Hadley cell contributions, both of which vanish at the poles. Since $E' - P' \propto dF_q'/dx$, these boundary conditions imply that the eddies and Hadley cell independently satisfy the conservation law that $E' = P'$ in the global mean.

Now suppose that the HS06 approximation was correct, such that the fractional change in $E - P$ was equal to $\alpha T'$ everywhere. Because of polar amplification, the eddy component of $E' - P'$ in this scenario would have a

larger magnitude where $E' < P'$ (at high latitudes) than where $E' > P'$ (in the subtropics), implying (impossibly) that $E' \neq P'$ in the global mean. The second term in Eq. (16) therefore represents a necessary correction to the HS06 approximation in the presence of polar amplification, without which the global water budget would not close. Because of downgradient energy transport, this correction will tend to be concentrated in midlatitudes where F_q is greatest, thereby causing the region over which $E - P > 0$ to expand, and shifting the latitude of minimum $E - P$ poleward. While these changes in the hydrologic cycle are often attributed to dynamical changes within the Hadley cell (Lu et al. 2007) and midlatitude storm tracks (HS06; Lu et al. 2010), this result suggests that downgradient energy transport may provide a complementary—and perhaps more fundamental—explanation.

b. *Connecting intermodel variability in $E' - P'$ to the spatial pattern of climate feedbacks*

In GCMs, R_f, G', and λ are not spatially uniform, as we assumed in section 3a. Roe et al. (2015) showed that spatial structure in these variables can have a significant impact on the pattern of surface warming, including the magnitude of polar amplification. Here we investigate the effect of such spatial structure on the profile of $E' - P'$ predicted by CMIP5 GCMs in response to abrupt CO_2 forcing. To minimize the influence of natural variability, we focus on years 126–150 after CO_2 is quadrupled, which represent the last 25 years of most GCM simulations. However, we have repeated our analysis using other time periods, with similar results in each case.

For each model, we estimate $G'(x)$ from the net change in surface energy fluxes, and $R_f(x)$ and $\lambda(x)$ as the y intercept and slope, respectively, of the regression line relating the time series of annual-mean surface temperature to the net radiation at the top of the atmosphere (Gregory et al. 2004). While this method may be less accurate than estimating $R_f(x)$ and $\lambda(x)$ from fixed SST simulations with and without increased CO_2, we find that the two methods produce very similar results in all models for which fixed SST simulations are available. We therefore choose the regression method because it allows us to include more models in our analysis.[2]

Figure 5a shows the average profile of $R_f(x)$, $G'(x)$, and $\lambda(x)$ in the ensemble mean of the CMIP5 simulations, while Figs. 5b and 5c show the resulting patterns of T' and $E' - P'$ from both the MEBM (red) and the GCMs (blue). In Fig. 5c, the vertical green lines indicate

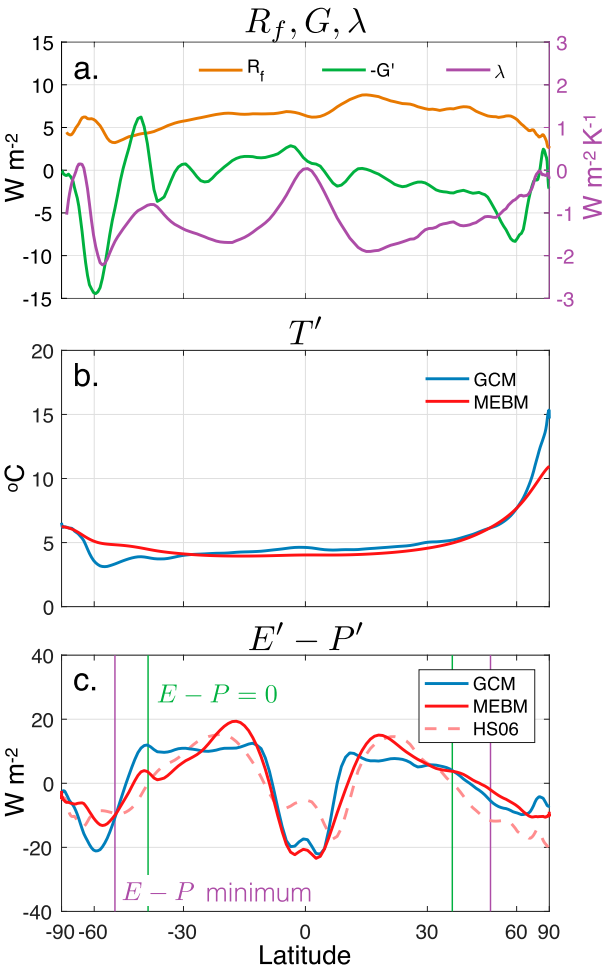

FIG. 5. (a) R_f (orange), change in G' (green; opposite sign), and λ (purple; W m^{-2} K^{-1}; as indicated by the right y axis) in the ensemble mean of 20 CMIP5 simulations of abrupt CO_2 quadrupling. (b) The zonal-mean profile of surface warming averaged over years 126–150 after CO_2 quadrupling in the CMIP5 ensemble mean (blue) and the MEBM (red). (c) The change in $E - P$ in the CMIP5 ensemble mean (blue) and the MEBM (red). The dashed red line represents the HS06 approximation. The vertical green (purple) lines indicate the highest latitude where $E - P = 0$ ($E - P$ has a local minimum) in the preindustrial GCM simulations.

the highest latitudes where $E - P = 0$ in the preindustrial GCM simulations, marking the poleward edge of the subtropics (Fig. 1). The extratropical minimum of $E - P$ is represented by a vertical purple line, which we interpret as a rough measure of the climatological storm-track position.

With respect to surface warming (Fig. 5b), the MEBM solution captures much of the large-scale structure of the GCM solution, including its hemispheric asymmetry, though it underpredicts the magnitude of polar amplification in the Northern Hemisphere by almost 4 K at the pole (14.7 vs 11.0 K). Similarly, for $E' - P'$ (Fig. 5c),

[2] The names of the models included in our analysis are listed above the panels in Fig. 6.

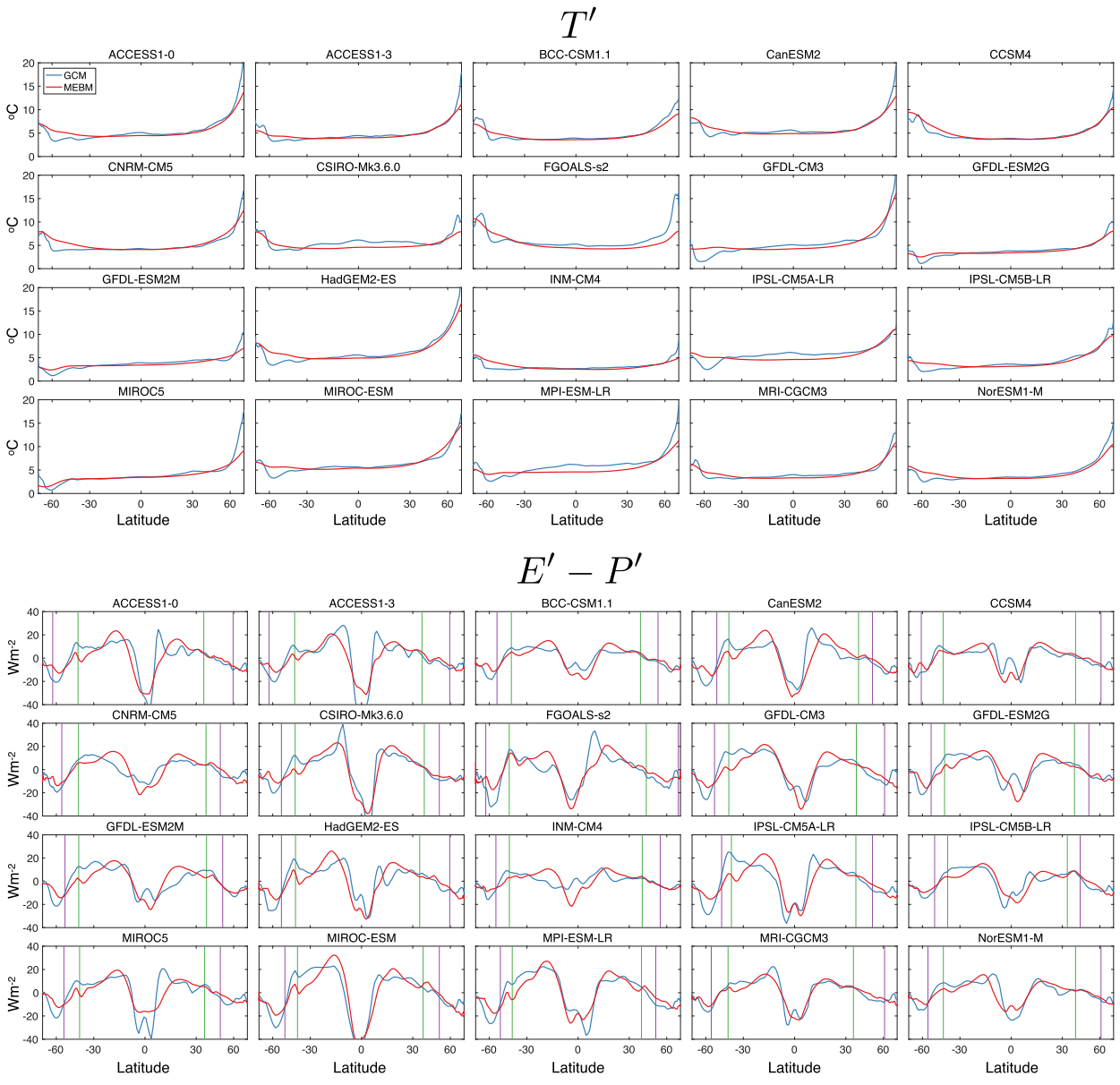

FIG. 6. As in Figs. 5b,c, but for each of the 20 CMIP5 ensemble members included in our analysis. (top) Surface warming and (bottom) the change in $E - P$.

the MEBM captures much of the overall response in the GCMs, including a poleward shift in both the subtropical boundary (Fig. 5c, green lines) and the extratropical $E - P$ minimum (Fig. 5c, purple lines). But here, too, the MEBM is imperfect: in the Southern Hemisphere, in particular, the magnitude of the poleward shift is too weak, suggesting that diffusion of near-surface moist static energy does not by itself explain the total change in zonal-mean $E - P$ in this region. Yet compared with the HS06 approximation (Fig. 5c, dashed line), the MEBM solution represents a clear improvement, highlighting the importance of spatial variations in R_f, λ, G', and T' in determining the response of the zonal-mean hydrologic cycle to global warming.

When the full ensemble of CMIP5 simulations is considered (Fig. 6), it is clear that the spatial patterns of R_f, G', and λ affect the detail of the climate response, but not the main features (e.g., polar amplification, wetter deep tropics, drier subtropics, and wetter high latitudes), indicating a high degree of agreement among models in these basic responses. Even so, the MEBM captures much of the intermodel variability in both T' (Fig. 6, top) and $E' - P'$ (Fig. 6, bottom) in response to differences in R_f, G', and λ. A quantitative assessment of the

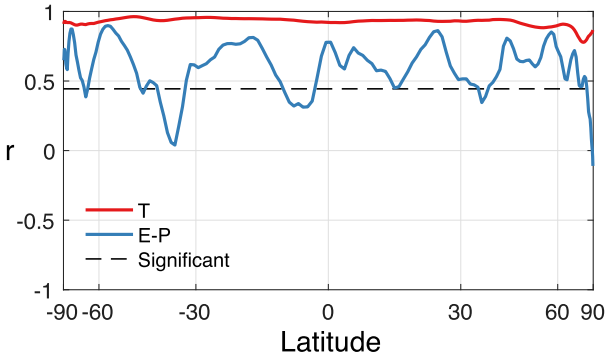

FIG. 7. The Pearson correlation coefficient at each latitude between GCM and MEBM solutions across the 20 CMIP5 ensemble members: T' (red line), $E' - P'$ (blue line), and the threshold for statistical significance at the 95% confidence level (dashed line; $r = 0.44$, 18 degrees of freedom).

MEBM's skill is presented in Fig. 7, which shows the correlation coefficient between the GCM and MEBM values of T' (red) and $E' - P'$ (blue) as a function of latitude. The dashed black line represents the threshold for statistical significance at the 95% confidence level ($r = 0.44$). With T' (Fig. 7, red), we find high correlations at all latitudes, with a global-mean value of $r = 0.90$. Although the correlations are somewhat weaker in polar regions of the Northern Hemisphere ($r \approx 0.6$–0.8), they remain well above the threshold of statistical significance everywhere. In the case of $E' - P'$ (Fig. 7, blue), the correlations are also strong in most regions ($r = 0.61$ in the global mean), and are statistically significant over 87% of the globe. These results imply that much of the intermodel differences in the zonal-mean response of the hydrologic cycle to global warming can be explained by the principle of downgradient energy transport applied to different patterns of forcing, feedbacks, and ocean heat uptake.

c. *Partitioning $E' - P'$ into E' and P'*

Because the MEBM only simulates energy transport and convergence, its solution for $E' - P'$ implies nothing about P'. However, if E' can be determined independently, the solution for P' can then be found as the difference between E' and $E' - P'$.

In their paper, HS06 assumed that E' was simply proportional to E, with a spatially uniform scaling factor equal to the fractional change in global-mean evaporation with global warming ($\sim 2\%\ \mathrm{K}^{-1}$). This approximation is shown in Fig. 8 (dashed line), along with the actual profile of E' taken from the ensemble mean of the CMIP5 simulations (blue line). Comparing the two curves, we find that the HS06 approximation captures the overall structure and magnitude of E' reasonably

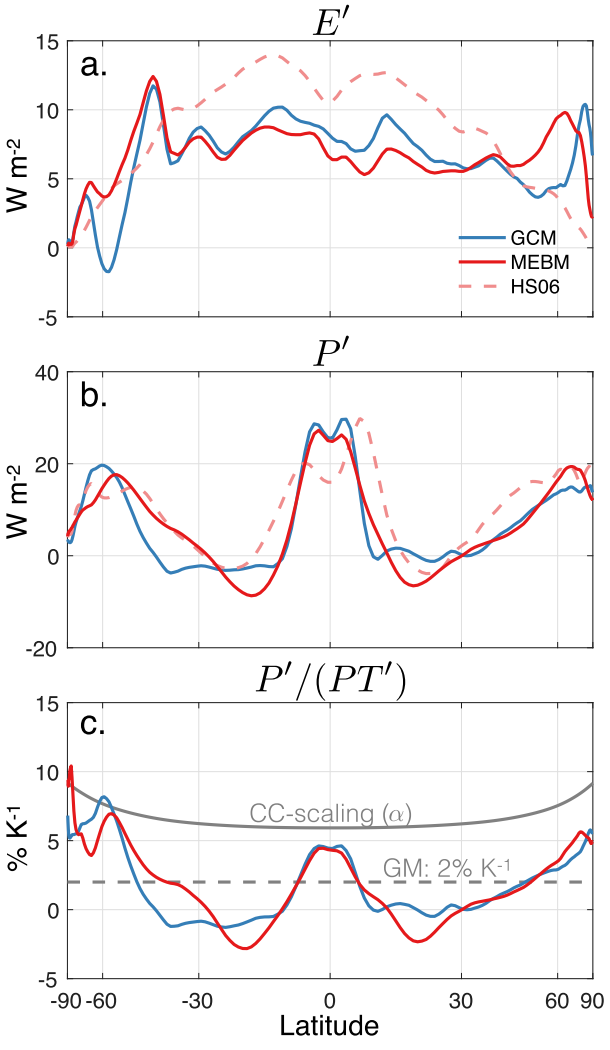

FIG. 8. (a) The change in zonal-mean evaporation in the CMIP5 ensemble mean (blue) and the MEBM (red), given by Eq. (17) assuming $R'_s = 0$. The dashed red line represents the HS06 approximation. (b) As in (a), but for zonal-mean precipitation, which was computed by subtracting the profiles of $E' - P'$ in Fig. 5c from the profiles of E' in (a). (c) The fractional change in precipitation per degree of local surface warming. The solid gray line represents Clausius–Clapeyron scaling [Eq. (11)], and the dashed gray line at $2\%\ \mathrm{K}^{-1}$ approximates the global-mean change predicted by GCMs.

well, but is too large in the tropics, and misses almost all of the regional-scale variations found in the GCM simulations.

A more accurate estimate of E' can be obtained using the surface energy approach of Siler et al. (2018). Building on earlier work by Penman (1948) and Monteith (1981), Siler et al. (2018) combine the surface energy budget with the bulk transfer equations for latent and sensible heat flux to arrive at a single expression for the change in surface evaporation with warming. Over the

oceans, where most global evaporation occurs, the change in evaporation can be approximated as

$$E' \approx \frac{ET'\beta_0(\alpha - 2/T) + R_s' - G'}{1 + \beta_0}, \tag{17}$$

where R_s' is the change in net radiation at the surface, $\beta_0(T)$ is the Bowen ratio in the limit of a saturated near-surface atmosphere, and all other variables are as defined previously. In the same CMIP5 simulations we analyze here, Siler et al. (2018) found that the first term on the rhs of Eq. (17) was the most important globally, while G' was identified as a leading control on the spatial pattern of E'. Meanwhile, R_s' was found to play a secondary role on both regional and global scales, and thus we choose to neglect it here. For E, we use the CMIP5 ensemble mean. All other variables in Eq. (17) can be determined from existing input (G') or output (T' and T), allowing us to solve for E' (and thus P') without adding any variables or complexity to the MEBM.

The red line in Fig. 8a shows the profile of E' given by Eq. (17), with $R_s' = 0$. Compared with the HS06 approximation (dashed line), Eq. (17) is more accurate at most latitudes, and also captures many of the regional variations in E' that are absent from the HS06 approximation. Taking the difference between E' and $E' - P'$ (Fig. 5c) yields P', which is shown in Fig. 8b for the CMIP5 ensemble (blue), the HS06 approximation (dashed line), and our MEBM solution (red line). As with E' and $E' - P'$, the MEBM solution for P' represents a substantial improvement over the HS06 approximation at most latitudes. This is particularly true in the tropics, where the MEBM successfully captures the large increase in precipitation near the equator, consistent with a narrowing of the ITCZ that has been attributed in part to the enhanced pole–equator gradient in moist static energy (Byrne and Schneider 2016). Elsewhere, the MEBM shows a decrease in subtropical precipitation and a large increase at high latitudes, which is also broadly consistent with GCM simulations. This agreement suggests that projected changes in zonal-mean precipitation are largely a consequence of constraints on atmospheric energy transport and surface fluxes, modulated by spatial variations in radiative forcing, feedbacks, and ocean heat uptake.

Figure 8c shows the same precipitation changes as Fig. 8b, but as a percentage change per degree of local warming. The gray dashed line in Fig. 8c represents the global-mean increase of $2\%\ \mathrm{K}^{-1}$, while the solid gray line represents the larger Clausius–Clapeyron rate of increase in atmospheric water vapor under constant relative humidity [α; Eq. (11)]. The MEBM emulates well the overall magnitude and pattern of the sensitivity of the GCM ensemble mean, albeit with notable mismatches in the subtropics and Southern Hemisphere midlatitudes. In the deep tropics and high latitudes, increases in latent heat flux convergence drive increases in precipitation that significantly exceed the global-mean sensitivity of $2\%\ \mathrm{K}^{-1}$, approaching or even exceeding the Clausius–Clapeyron rate at some latitudes. In the subtropics, meanwhile, the change in precipitation is small and/or negative, allowing the global-mean value of $2\%\ \mathrm{K}^{-1}$ to be maintained. Significantly, this spatial pattern of precipitation sensitivity in the MEBM does not require knowledge of the specific mechanisms (e.g., stratiform or convective processes) generating the precipitation; everywhere, the precipitation change is simply the result of global energetic and transport constraints.

4. Discussion

In this paper, we have incorporated a new Hadley cell parameterization into an existing moist static energy balance model (MEBM), and used it to investigate the implications of downgradient energy transport for the response of the zonal-mean hydrologic cycle to global warming. In the idealized case of spatially uniform radiative forcing and feedbacks, we found that downgradient energy transport implies a poleward expansion of the subtropics, where $E - P > 0$, and a poleward shift in the extratropical minimum of $E - P$, which is consistent with a change in storm-track latitude. We showed that both of these phenomena are tied to polar-amplified warming in the MEBM, which is itself closely tied to downgradient energy transport (Roe et al. 2015). When forced with realistic patterns of forcing, feedbacks, and ocean heat uptake from comprehensive GCMs, the MEBM was found to broadly replicate the simulated changes in $E - P$, while also capturing much of the intermodel variability across the CMIP5 ensemble. Given the surface energy constraints on evaporation change, the MEBM predicts changes in zonal-mean precipitation that are also consistent with GCM projections, including a decrease in subtropical precipitation and a contraction and intensification of the ITCZ.

There are surely ways to make the MEBM more realistic—for example, by allowing D to vary with latitude or climate state, or adjusting $w(x)$ to include Ferrel and polar cells. However, in experimenting with such modifications, we have found that their impact on $E' - P'$ is generally small. For example, when we increase D by 20% in the global warming simulation, $E' - P'$ changes by less than $2.5\ \mathrm{W\,m^{-2}}$ at all latitudes. Similarly, when we add a Ferrel cell to the MEBM [$w(x) = \cos(\pi x)(1 - |x|)$], the change in $E' - P'$ is less than $3\ \mathrm{W\,m^{-2}}$ everywhere. In

both cases, the changes result in better agreement with GCMs in the Southern Hemisphere midlatitudes, but the improvement is modest relative to existing differences of about $10\,\mathrm{W\,m^{-2}}$ between the MEBM and GCM solutions in this region (Fig. 5c).

Another question to consider is the extent to which the spatial patterns of local feedbacks λ and the change in ocean heat uptake G' are truly independent of atmospheric heat and moisture transport, as we have assumed here. While the spatial pattern of G' is set by regional ocean circulations (Marshall et al. 2015; Armour et al. 2016), it seems plausible that its magnitude may be, in part, set by the magnitude of local atmospheric heat flux convergence. Likewise, there is evidence that λ depends on the spatial pattern of surface warming within GCMs (Rose et al. 2014; Andrews and Webb 2018; Po-Chedley et al. 2018). An interesting avenue of future research would be to evaluate these interactions with the MEBM coupled to a dynamic ocean while allowing for local feedbacks to vary with the pattern of warming.

Finally, our results raise interesting questions about the influence of atmospheric dynamical changes on the zonal-mean hydrologic cycle. From mixing length theory, our assumption of fixed diffusivity D is equivalent to assuming that changes in eddy dynamics are negligible (e.g., Frierson et al. 2007). Moreover, as implemented here [Eq. (6)], the MEBM does not account for possible changes in the partitioning between eddy and Hadley cell energy transport that might result from dynamical changes. Yet despite these simplifications, the MEBM gives changes in $E - P$ that are consistent with poleward shifts in the storm tracks and subtropics—responses that have previously been attributed to dynamical changes in the eddies and Hadley cell (e.g., HS06; Lu et al. 2007; Scheff and Frierson 2012). Further study is needed to better understand the relationship between such dynamical changes and downgradient energy transport (e.g., Tandon et al. 2013; Mbengue and Schneider 2017, 2018). Even without invoking dynamical changes, however, our study shows that the principle of downgradient energy transport provides a simple explanation for many aspects of the zonal-mean hydrologic cycle and its simulated response to global warming.

Acknowledgments. We are grateful to Spencer Hill and two anonymous reviewers for their excellent comments. We also acknowledge the important contribution of Marcia Baker, who first proposed the idea of modifying the MEBM to include a realistic hydrologic cycle. KCA's contribution was funded by the National Science Foundation (AGS-1752796).

APPENDIX

Estimating the Change in Diffusive Latent Heat Transport with Warming

In the original MEBM, latent heat is transported downgradient with the same diffusivity as total moist static energy [Eq. (2)]:

$$F_q(x) = -\frac{2\pi p_s}{g} D(1-x^2) L \frac{dq}{dx}. \tag{A1}$$

According to the Clausius–Clapeyron equation

$$\frac{dq}{dT} = \alpha q, \tag{A2}$$

the meridional moisture gradient in Eq. (A1) is strongly dependent on the meridional temperature gradient

$$\frac{dq}{dx} = \alpha q \frac{dT}{dx}. \tag{A3}$$

Substituting Eq. (A3) into Eq. (A1) and differentiating yields the change in northward latent heat flux

$$F_q'(x) \approx -\frac{2\pi p_s}{g} D(1-x^2) L \left[T' \frac{d(\alpha q)}{dT} \frac{dT}{dx} + \alpha q \frac{dT'}{dx} \right], \tag{A4}$$

which simplifies to Eq. (14).

REFERENCES

Andrews, T., and M. J. Webb, 2018: The dependence of global cloud and lapse rate feedbacks on the spatial structure of tropical Pacific warming. *J. Climate*, **31**, 641–654, https://doi.org/10.1175/JCLI-D-17-0087.1.

Armour, K. C., J. Marshall, J. R. Scott, A. Donohoe, and E. R. Newsom, 2016: Southern Ocean warming delayed by circumpolar upwelling and equatorward transport. *Nat. Geosci.*, **9**, 549–554, https://doi.org/10.1038/ngeo2731.

Budyko, M. I., 1969: The effect of solar radiation variations on the climate of the Earth. *Tellus*, **21** (5), 611–619, https://doi.org/10.3402/tellusa.v21i5.10109.

Byrne, M. P., and T. Schneider, 2016: Narrowing of the ITCZ in a warming climate: Physical mechanisms. *Geophys. Res. Lett.*, **43**, 11 350–11 357, https://doi.org/10.1002/2016GL070396.

Donohoe, A., J. Marshall, D. Ferreira, and D. McGee, 2013: The relationship between ITCZ location and cross-equatorial atmospheric heat transport: From the seasonal cycle to the Last Glacial Maximum. *J. Climate*, **26**, 3597–3618, https://doi.org/10.1175/JCLI-D-12-00467.1.

——, ——, ——, K. Armour, and D. McGee, 2014: The interannual variability of tropical precipitation and interhemispheric energy transport. *J. Climate*, **27**, 3377–3392, https://doi.org/10.1175/JCLI-D-13-00499.1.

Flannery, B. P., 1984: Energy balance models incorporating transport of thermal and latent energy. *J. Atmos. Sci.*,

41, 414–421, https://doi.org/10.1175/1520-0469(1984)041<0414:EBMITO>2.0.CO;2.

Frierson, D. M. W., and Y.-T. Hwang, 2012: Extratropical influence on ITCZ shifts in slab ocean simulations of global warming. *J. Climate*, **25**, 720–733, https://doi.org/10.1175/JCLI-D-11-00116.1.

——, I. M. Held, and P. Zurita-Gotor, 2007: A gray-radiation aquaplanet moist GCM. Part II: Energy transports in altered climates. *J. Atmos. Sci.*, **64**, 1680–1693, https://doi.org/10.1175/JAS3913.1.

——, and Coauthors, 2013: Contribution of ocean overturning circulation to tropical rainfall peak in the Northern Hemisphere. *Nat. Geosci.*, **6**, 940–944, https://doi.org/10.1038/ngeo1987.

Gregory, J. M., and Coauthors, 2004: A new method for diagnosing radiative forcing and climate sensitivity. *Geophys. Res. Lett.*, **31**, L03205, https://doi.org/10.1029/2003GL018747.

Hartmann, D. L., 1994: *Global Physical Climatology*. International Geophysics Series, Vol. 56, Academic Press, 411 pp.

Held, I. M., 2001: The partitioning of the poleward energy transport between the tropical ocean and atmosphere. *J. Atmos. Sci.*, **58**, 943–948, https://doi.org/10.1175/1520-0469(2001)058<0943:TPOTPE>2.0.CO;2.

——, and B. J. Soden, 2006: Robust responses of the hydrological cycle to global warming. *J. Climate*, **19**, 5686–5699, https://doi.org/10.1175/JCLI3990.1.

Hill, S. A., Y. Ming, and I. M. Held, 2015: Mechanisms of forced tropical meridional energy flux change. *J. Climate*, **28**, 1725–1742, https://doi.org/10.1175/JCLI-D-14-00165.1.

Hwang, Y.-T., and D. M. W. Frierson, 2010: Increasing atmospheric poleward energy transport with global warming. *Geophys. Res. Lett.*, **37**, L24807, https://doi.org/10.1029/2010GL045440; Corrigendum, **38**, L09801, https://doi.org/10.1029/2011GL047604.

——, and ——, 2013: Link between the double-intertropical convergence zone problem and cloud biases over the Southern Ocean. *Proc. Natl. Acad. Sci. USA*, **110**, 4935–4940, https://doi.org/10.1073/pnas.1213302110.

——, ——, and S. M. Kang, 2013: Anthropogenic sulfate aerosol and the southward shift of tropical precipitation in the late 20th century. *Geophys. Res. Lett.*, **40**, 2845–2850, https://doi.org/10.1002/grl.50502.

Kang, S. M., I. M. Held, D. M. W. Frierson, and M. Zhao, 2008: The response of the ITCZ to extratropical thermal forcing: Idealized slab-ocean experiments with a GCM. *J. Climate*, **21**, 3521–3532, https://doi.org/10.1175/2007JCLI2146.1.

Lu, J., G. A. Vecchi, and T. Reichler, 2007: Expansion of the Hadley cell under global warming. *Geophys. Res. Lett.*, **34**, L06805, https://doi.org/10.1029/2006GL028443; Corrigendum, **34**, L14808, https://doi.org/10.1029/2007GL030931.

——, G. Chen, and D. M. W. Frierson, 2010: The position of the midlatitude storm track and eddy-driven westerlies in aquaplanet AGCMs. *J. Atmos. Sci.*, **67**, 3984–4000, https://doi.org/10.1175/2010JAS3477.1.

Marshall, J., A. Donohoe, D. Ferreira, and D. McGee, 2014: The ocean's role in setting the mean position of the inter-tropical convergence zone. *Climate Dyn.*, **42**, 1967–1979, https://doi.org/10.1007/s00382-013-1767-z.

——, J. R. Scott, K. C. Armour, J.-M. Campin, M. Kelley, and A. Romanou, 2015: The ocean's role in the transient response of climate to abrupt greenhouse gas forcing. *Climate Dyn.*, **44**, 2287–2299, https://doi.org/10.1007/s00382-014-2308-0.

Mbengue, C., and T. Schneider, 2017: Storm-track shifts under climate change: Toward a mechanistic understanding using baroclinic mean available potential energy. *J. Atmos. Sci.*, **74**, 93–110, https://doi.org/10.1175/JAS-D-15-0267.1.

——, and ——, 2018: Linking Hadley circulation and storm tracks in a conceptual model of the atmospheric energy balance. *J. Atmos. Sci.*, **75**, 841–856, https://doi.org/10.1175/JAS-D-17-0098.1.

Merlis, T. M., T. Schneider, S. Bordoni, and I. Eisenman, 2013: Hadley circulation response to orbital precession. Part I: Aquaplanets. *J. Climate*, **26**, 740–753, https://doi.org/10.1175/JCLI-D-11-00716.1.

Monteith, J. L., 1981: Evaporation and surface temperature. *Quart. J. Roy. Meteor. Soc.*, **107**, 1–27, https://doi.org/10.1002/qj.49710745102.

Neelin, J. D., and I. M. Held, 1987: Modeling tropical convergence based on the moist static energy budget. *Mon. Wea. Rev.*, **115**, 3–12, https://doi.org/10.1175/1520-0493(1987)115<0003:MTCBOT>2.0.CO;2.

North, G. R., 1975: Theory of energy-balance climate models. *J. Atmos. Sci.*, **32**, 2033–2043, https://doi.org/10.1175/1520-0469(1975)032<2033:TOEBCM>2.0.CO;2.

Peixoto, J., and A. H. Oort, 1996: The climatology of relative humidity in the atmosphere. *J. Climate*, **9**, 3443–3463, https://doi.org/10.1175/1520-0442(1996)009<3443:TCORHI>2.0.CO;2.

Penman, H. L., 1948: Natural evaporation from open water, bare soil and grass. *Proc. Roy. Soc. London*, **193**, 120–145, https://doi.org/10.1098/rspa.1948.0037.

Pierrehumbert, R. T., 2010: *Principles of Planetary Climate*. Cambridge University Press, 652 pp.

Po-Chedley, S., K. C. Armour, C. M. Bitz, M. D. Zelinka, B. D. Santer, and Q. Fu, 2018: Sources of intermodel spread in the lapse rate and water vapor feedbacks. *J. Climate*, **31**, 3187–3206, https://doi.org/10.1175/JCLI-D-17-0674.1.

Roe, G. H., N. Feldl, K. C. Armour, Y.-T. Hwang, and D. M. W. Frierson, 2015: The remote impacts of climate feedbacks on regional climate predictability. *Nat. Geosci.*, **8**, 135–139, https://doi.org/10.1038/ngeo2346.

Rose, B. E. J., K. C. Armour, D. S. Battisti, N. Feldl, and D. D. B. Koll, 2014: The dependence of transient climate sensitivity and radiative feedbacks on the spatial pattern of ocean heat uptake. *Geophys. Res. Lett.*, **41**, 1071–1078, https://doi.org/10.1002/2013GL058955.

Scheff, J., and D. Frierson, 2012: Twenty-first-century multimodel subtropical precipitation declines are mostly midlatitude shifts. *J. Climate*, **25**, 4330–4347, https://doi.org/10.1175/JCLI-D-11-00393.1.

Sellers, W. D., 1969: A global climatic model based on the energy balance of the earth-atmosphere system. *J. Appl. Meteor.*, **8**, 392–400, https://doi.org/10.1175/1520-0450(1969)008<0392:AGCMBO>2.0.CO;2.

Siler, N., G. H. Roe, K. C. Armour, and N. Feldl, 2018: Revisiting the surface-energy-flux perspective on the sensitivity of global precipitation to climate change. *Climate Dyn.*, https://doi.org/10.1007/s00382-018-4359-0, in press.

Tandon, N. F., E. P. Gerber, A. H. Sobel, and L. M. Polvani, 2013: Understanding Hadley cell expansion versus contraction: Insights from simplified models and implications for recent observations. *J. Climate*, **26**, 4304–4321, https://doi.org/10.1175/JCLI-D-12-00598.1.